A Threonine Stabilizes the NiC and NiR Catalytic Intermediates of [NiFe]-hydrogenase.

Abbas Abou-Hamdan, Pierre Ceccaldi, Hugo Lebrette, Oscar Gutiérrez-Sanz, Pierre Richaud, Laurent Cournac, Bruno Guigliarelli, Antonio L de Lacey, Christophe Léger, Anne Volbeda, et al.

THE JOURNAL OF BIOLOGICAL CHEMISTRY VOL. 290, NO. 13, pp. 8550–8558, March 27, 2015

A Threonine Stabilizes the NiC and NiR Catalytic Intermediates of [NiFe]-hydrogenase*

Received for publication, December 8, 2014, and in revised form, February 6, 2015 Published, JBC Papers in Press, February 9, 2015, DOI 10.1074/jbc.M114.630491

Abbas Abou-Hamdan[‡1], Pierre Ceccaldi[‡], Hugo Lebrette[§2], Oscar Gutiérrez-Sanz[¶], Pierre Richaud[‖‡‡], Laurent Cournac[‖**‡‡3], Bruno Guigliarelli[‡], Antonio L. De Lacey[¶], Christophe Léger[‡], Anne Volbeda[§], Bénédicte Burlat[‡], and Sébastien Dementin[‡4]**

*From the [‡]Laboratoire de Bioénergétique et Ingénierie des Protéines, Institut de Microbiologie de la Méditerranée, UMR 7281 Aix-Marseille Université/CNRS, 31 Chemin J. Aiguier, 13402 Marseille Cedex 20, France, [§]Metalloproteins Unit, Institut de Biologie Structurale, UMR 5075 Commissariat à l'Energie Atomique/CNRS/Université Joseph Fourier, 6 rue Jules Horowitz, 38000, Grenoble, France, [¶]Instituto de Catálisis y Petroleoquímica, Consejo Superior de Investigaciones Científicas, c/Marie Curie 2, L10, 28049 Madrid, Spain, [‖]Laboratoire de Bioénergétique et Biotechnologie des Bactéries et Microalgues, Commissariat à l'Energie Atomique, Direction des Sciences du Vivant, Institut de Biologie Environnementale et Biotechnologie, Saint-Paul-lez-Durance, F-13108, France, **CNRS, UMR 7265 Biologie Végétale et Microbiologie Environnementale (BVME), Saint-Paul-lez-Durance, 13108, France, and [‡‡]Aix-Marseille Université, BVME UMR7265, Marseille F-13284, France*

Background: A conserved threonine in [NiFe]-hydrogenases is a putative proton transfer relay.
Results: Poorly active variants have modified spectroscopic signatures associated with changes in local protein structure.
Conclusion: This threonine is not necessarily a proton transfer relay but, rather, stabilizes reaction intermediates.
Significance: Combined kinetic, spectroscopic, and structural characterizations of several variants are necessary to assess the role of a residue in [NiFe]-hydrogenase.

The heterodimeric [NiFe] hydrogenase from *Desulfovibrio fructosovorans* catalyzes the reversible oxidation of H_2 into protons and electrons. The catalytic intermediates have been attributed to forms of the active site (NiSI, NiR, and NiC) detected using spectroscopic methods under potentiometric but non-catalytic conditions. Here, we produced variants by replacing the conserved Thr-18 residue in the small subunit with Ser, Val, Gln, Gly, or Asp, and we analyzed the effects of these mutations on the kinetic (H_2 oxidation, H_2 production, and H/D exchange), spectroscopic (IR, EPR), and structural properties of the enzyme. The mutations disrupt the H-bond network in the crystals and have a strong effect on H_2 oxidation and H_2 production turnover rates. However, the absence of correlation between activity and rate of H/D exchange in the series of variants suggests that the alcoholic group of Thr-18 is not necessarily a proton relay. Instead, the correlation between H_2 oxidation and production activity and the detection of the NiC species in reduced samples confirms that NiC is a catalytic intermediate and suggests that Thr-18 is important to stabilize the local protein structure of the active site ensuring fast NiSI-NiC-NiR interconversions during H_2 oxidation/production.

[NiFe]-hydrogenases catalyze the multistep, reversible reaction of H_2 oxidation. The catalytic cycle involves H_2 transport through a dedicated tunnel network to a buried [NiFe] active site where heterolytic cleavage occurs to produce protons and electrons (Fig. 1*A*). When purified aerobically, the so-called "standard" heterodimeric [NiFe] enzymes from the *Desulfovibrio* genus are inactive and can be activated by reduction. Using EPR or FTIR, the inactive sample appears as a mixture of two forms called NiA and NiB (1–3). The proposed catalytic cycle of the enzymes involves three intermediates (NiSI, NiC, and NiR) that have only been detected under non-catalytic conditions (2, 4). The most commonly accepted mechanism suggests that H_2 binds the nickel ion in the NiSI state to yield NiR (both are in the Ni(II) state) (5). NiR would contain a Ni-Fe bridging hydride ligand. This state is oxidized to NiSI in a two-step process, with NiC being an intermediate in the Ni(III) state and also with a putative bridging hydride (Fig. 1*B*) (2, 3). NiSI and NiR are observed in different protonation states ($NiSI_I$ and $NiSI_{II}$; NiR_I and NiR_{II}) (2, 6). A NiR_{III} state has also been detected in *Allochromatium vinosum* hydrogenase (noted Ni_a-SR_{1913}) (7) and attributed to a NiR state with two fewer protons than NiR_I (8). NiL, a state observed upon irradiation of NiC, is sometimes seen as a putative reaction intermediate as proposed for Hyd-1 from *Escherichia coli* in which NiC could not be detected (9).

In [NiFe]-hydrogenases, the electrons produced at the active site are transferred to the redox partner at the protein surface via a chain of three FeS clusters called proximal, medial, and

* This work was supported by the CNRS, the Agence Nationale de la Recherche (HYLIOX and HEROS projects: ANR-07-BIOE-010 and ANR-14-CE05-0010), the Aix-Marseille Université, and the City of Marseilles. This work was also supported by grants from the CNRS and the Région Provence-Alpes Côte d'Azur (to A. A.-H.), the Spanish MINECO CTQ2012-32448 project (A. L. D. L.), the Spanish FPI program (to O. G.-S.), the Commissariat à l'Energie Atomique et aux Energies Alternatives (CEA), and the CNRS (to H. L. and A. V.).
The atomic coordinates and structure factors (codes 4UCW, 4UCX, and 4UCQ) have been deposited in the Protein Data Bank (http://wwpdb.org/).
[1] Present address: Institut Cochin, INSERM U1016-CNRS UMR8104-Université Paris Descartes, Faculté de Médecine, 24, rue du Faubourg Saint-Jacques, 75014 Paris, France.
[2] Present address: Dept. of Biochemistry and Biophysics, Stockholm University, Svante Arrhenius väg 16C, SE-106 91 Stockholm, Sweden.
[3] Present address: IRD, UMR Eco&Sols, Bat 12, 2 Place Viala, 34060 Montpellier Cedex 2, France.
[4] To whom correspondence should be addressed. E-mail: dementin@imm.cnrs.fr.

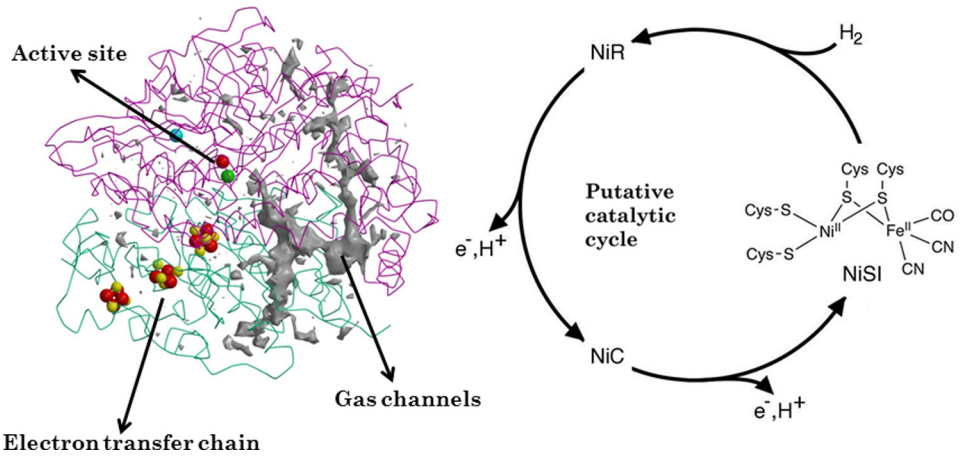

FIGURE 1. *A*, structure of the heterodimeric [NiFe]-hydrogenase from *D. fructosovorans* (PDB accession code 1YWQ). The large subunit (*purple*) contains the [NiFe] cluster. H_2 accesses to or escapes from the active site through hydrophobic gas channels. The electrons are transferred to or from the active site via a chain made of three FeS clusters in the small subunit (*cyan*). The proximal and distal clusters are [4Fe4S] clusters, and the medial cluster is a [3Fe4S] cluster. *B*, putative catalytic cycle involving states (NiSI, NiR, and NiC) observed by spectroscopy under non-catalytic conditions.

distal clusters (Fig. 1*A*). The protons are transferred to the solvent along pathways that consist of water molecules and protonatable amino acid side chains, most of which still remain elusive. Identifying a proton transfer pathway in hydrogenase is a considerable task (10) because there is no experimental method that makes it possible to measure the rate of a single proton transfer, and one has to rely on site-directed mutagenesis and global measurements of turnover rates. Moreover, it is often impossible to make sure that a mutation only affects the putative proton transfer step of interest. Several proton pathways have nonetheless been proposed on the basis of crystallographic and theoretical studies (10–17). In standard [NiFe]-hydrogenases from *Desulfovibrio* species, some of the proposed pathways start with a Glu residue (Glu-25^L in the large subunit[5] of the *Desulfovibrio fructosovorans* (*Df*)[6] enzyme). An alternative pathway not involving this Glu and starting with an Arg is proposed in a study of the [NiFe] enzyme from *Thiocapsa roseopersicina* (17). The usual experimental approach for identifying proton transfer (PT) relays in [NiFe]-hydrogenases consists of exchanging residues with others whose side chain is not protonatable and measuring the H_2 production/oxidation, the *para*/*ortho* H_2 conversion, and the H/D exchange (HDE) activities of the mutated enzymes (18). The H_2 production/oxidation reactions involve H_2 intramolecular diffusion (in or out), H_2 splitting and oxidation at the active site, and H^+ and e^- transfers. The *para*/*ortho* reaction involves only H_2 diffusion, H_2 binding, splitting, and recombination at the active site and provides information on the ability of the active site to perform chemistry (18). Finally, the electron transfer-independent HDE activity reports on H_2 diffusion and on the ability of the active site to split H_2 into a heavy hydride and a deuteron and transfer the protons and deuterons to and from the solvent (19). It has been proposed that the enzyme interconverts between NiSI and NiR when catalyzing HDE (20, 21). A combination of these three assays has been used to investigate PT in hydrogenase (22, 23); for example, if a certain variant is affected in both H_2 production/oxidation and H/D exchange, but catalyzes the conversion between para and ortho H_2, then it is likely that the mutated residue is involved in PT. This approach was used to show that Glu-25^L in the large subunit of the enzyme from *Df* and Glu-13^L in the sensor enzyme from *Ralstonia eutropha* are essential for PT (22, 23). On the contrary, a variant with impaired H_2 production/oxidation but unaffected in *para*/*ortho* conversion and HDE activities is probably unable to rapidly transfer electrons to the redox partner, as observed for the D15^{L}H variant of the H_2 sensor in *R. eutropha* (23).

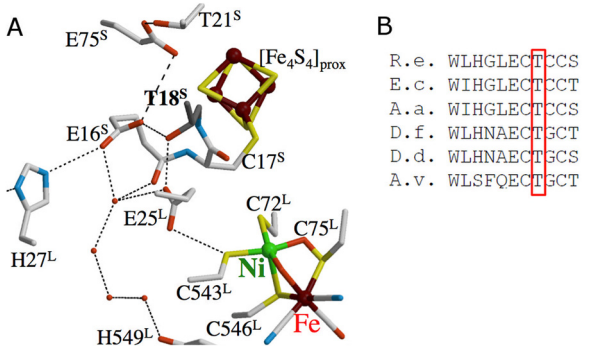

FIGURE 2. *A*, location of Thr-18^S in the crystal structure of WT *D. fructosovorans* [NiFe]-hydrogenase in the unready NiA/NiSU state (41). *B*, protein sequence alignment showing that Thr-18^S is conserved in [NiFe]-hydrogenases (*R.e.*, membrane-bound hydrogenase (*MBH*) from *R. eutropha*; *E.c.*, hydrogenase 1 from *E. coli*; *A.a.*, MBH from *Aquifex aeolicus*; *D.f.*, *D.d*, *A.v.*, soluble enzymes from *D. fructosovorans*, *Desulfovibrio desulfuricans*, and *A. vinosum*).

In this paper we focus on the conserved Thr-18^S residue in the small subunit of the *Df* [NiFe] hydrogenase (Fig. 2*B*). Recent calculations suggest it is a PT relay (14, 16), but alternative pathways that do not include Thr-18^S have also been proposed (14, 17). Moreover, the examination of the structure of the enzyme reveals that this residue is in a critical position; it is H-bonded to the first proton transfer residue Glu-25^L, it is near Cys-17^S (a ligand of the proximal FeS cluster), and its Cγ2 shapes the gas channel (Fig. 2*B*). This suggests that Thr-18^S may have other roles than transferring protons.

To address the role of Thr-18^S, we studied the kinetic (H_2 production/oxidation and HDE reactions), spectroscopic (EPR,

[5] A residue X is noted X^L or X^S when it is located in the large or in the small subunit, respectively.

[6] The abbreviations used are: *Df*, *D. fructosovorans*; PT, proton transfer; HDE, H/D exchange.

FTIR), and structural (x-ray crystallography) properties of variant enzymes in which Thr-18^S is replaced by residues that bear alcoholic (Ser), non-protonatable (Val, Gln, Gly), or protonatable (Asp) side chains.

EXPERIMENTAL PROCEDURES

Enzyme Production—The Strep-tagged WT and variant were constructed using bacterial strains, plasmids, growth conditions, site-directed mutagenesis strategy, and the enzyme purification protocol as described in references (24, 25). The aerobically purified WT enzyme exhibits a UV/visible spectrum of a non-heme protein with a broad absorption peak around 400 nm indicative of the three FeS clusters harbored by the small subunit. The purity index ($DO_{400\ nm}/DO_{280\ nm}$) of purified WT is 0.26–0.27, and it can be used to assess the presence of the FeS clusters in the variants (26). This value is 0.26–0.27 for the five variants, suggesting the correct incorporation of the three FeS clusters. This is supported by the EPR, FTIR, and crystallographic characterizations.

Kinetic Characterization—The H_2 oxidation activity of the enzymes was assayed spectrophotometrically using 50 mM methyl viologen as electron acceptor at pH 8 and 30 °C (25).

H_2 production was followed using mass spectrometry in a solution initially saturated with argon, with 2 mM reduced methyl viologen at pH 7.2 and 30 °C. The initial rates of H_2 production were extrapolated using a plot of 1/rate against $1/[H_2]$ as H_2 inhibits H_2 production (27, 28).

The HDE experiments were performed at pH 7.2 and 30 °C as described in Leroux *et al.* (25) and used to measure the rate of HDE and calculate the rate constant of H_2 release (k_{out}) and the first order rate constant of H/D exchange at the active site (k) as described in Abou-Hamdan *et al.* (19).

EPR and FTIR Spectroscopies—The EPR spectra were recorded on a Bruker ELEXSYS E500 spectrometer fitted with an Oxford Instruments ESR 900 helium flow cryostat. Quantifications were made by using an external standard solution of freshly prepared 1 mM Cu-EDTA in 100 mM Tris-HCl, 10 mM EDTA at pH 8 transferred into a calibrated EPR tube. Potentiometric titrations were performed as previously described (29). The infrared spectra were performed in a gas-tight transmission cell of CaF_2 as reported in Volbeda *et al.* (30).

X-ray Crystallographic Analyses—Crystals of the *Df* [NiFe]-hydrogenase T18D, T18V, and T18G variants were obtained at 20 °C either in an anaerobic glovebox or under air using the hanging drop vapor diffusion method, mixing 1.5 μl of protein solution with 1.5 μl of 17–20% polyethylene glycol 6000, 0.1–0.2 M MES, pH 6.0–6.3, reservoir solution. Concentrations of the protein solution were 9.15, 9.24, and 10.6 mg/ml for the T18D, T18V, and T18G variants, respectively. Monoclinic crystals with the usual $P2_1$ spacegroup with three hydrogenase heterodimers per asymmetric unit were typically obtained within 3 days (average cell dimensions: a, 62.9 Å; b, 99.6 Å; c, 182.4 Å, β 92.2°). All crystals were cryoprotected in the reservoir solution used for crystallization supplemented with 20% glycerol before they were flash-cooled in liquid nitrogen or in liquid propane (31). X-ray data were collected at the European Synchrotron Radiation Facility in Grenoble, France, and at the Swiss Light Source in Villigen, Switzerland. After data reduction and scaling with the XDS package (32), structures were solved by molecular replacement using PHASER (33), starting from the 1.8 Å resolution structure of the S499A variant (34). Next they were refined with REFMAC5 (35) using TLS bodies for the individual hydrogenase subunits. In addition, non-crystallographic symmetry restraints were used for the T18D variant. The atomic models were manually corrected where necessary with COOT (36). Averaged omit maps were used to resolve the structural consequences of the performed mutations (see Fig. 6, *B–D*). Table 1 lists the data and refinement statistics and PDB accession codes.

TABLE 1
Crystallographic statistics for *D. fructosovorans* [NiFe]-hydrogenase Thr-18^S variants

Variant	T18V	T18G	T18D
Crystal growth conditions	Anaerobic	Anaerobic	Aerobic
X-ray data			
Synchrotron	ESRF	SLS	ESRF
Beam line	ID14-2	X06SA	ID14-2
Detector	ADSC	Pilatus	ADSC
X-ray wavelength (Å)	0.9330	0.9763	0.9330
Resolution range (Å)	40-2.3	50-1.95	40-2.6
Unique reflections	92,096	160,613	70,368
Rsym (%)	7.3	4.2	7.2
$<I/\sigma>$	13.5	13.6	13.0
Data completeness (%)	93.5	99.2	99.2
High resolution shell (Å)	2.35-2.30	2.01-1.95	2.76-2.60
Unique reflections	4,142	13,832	11,371
Rsym (%)	26.0	37.0	35.7
$\langle I/\sigma \rangle$	3.9	2.3	3.4
Data completeness (%)	67.9	99.3	97.8
Refinement			
Resolution range (Å)	25.0-2.3	25.0-1.95	25-2.6
Reflections used for R_{work}	87,451	152,472	66,841
Reflections used for R_{free}	4,581	8,066	3,462
Number of atoms	19,144	19,172	19,012
R_{work} (%)	19.2	19.7	19.8
R_{free} (%)	23.6	23.1	24.2
σ_{bond} (Å)	0.012	0.013	0.015
σ_{angle} (°)	1.5	1.4	1.6
$\langle B \rangle$ (Å^2)	28.5	40.9	49.7
PDB deposition code	4UCW	4UCX	4UCQ

TABLE 2
Kinetic properties of the Thr-18^S variants
All activities are expressed in μmol.min^{-1}·mg^{-1}. ND, not determined. The errors are ±20%.

Enzyme	H_2 oxidation	H_2 production	HD exchange	H_2 release
			k	k_{out}
WT	330	80	700	1200
T18S	170	30	700	940
T18V	20	1	1	ND
T18Q	30	3	3	ND
T18G	5	2	270	1900
T18D	30	15	80	220

RESULTS

All Thr-18^S Mutations Affect H_2 Oxidation and Production Activities—The impact of mutations on the activities of the enzyme was assessed by measuring the rates of H_2 oxidation and H^+ reduction using methyl viologen as redox partner. As shown in Table 2, the T18S variant has approximatively half the activities of the WT, but the T18V, T18Q, T18G, and T18D variants very slowly oxidize H_2 (<10% activity compared with WT). Although the T18D mutation is less deleterious for H_2 production activity than the T18V, T18Q, and T18G mutations, our results show that the alcohol function is important

$$D_2 + 2H^+ \rightleftharpoons 2D^+ + H_2$$

$$D_{2(out)} \underset{k_{out}}{\overset{k_{in}}{\rightleftharpoons}} D_{2(in)} \xrightarrow[k]{H^+/D^+} HD_{(in)} \xrightarrow[k]{H^+/D^+} H_{2(in)} \underset{k_{in}}{\overset{k_{out}}{\rightleftharpoons}} H_{2(out)}$$

$$HD_{(in)} \underset{k_{out}}{\overset{k_{in}}{\rightleftharpoons}} HD_{(out)}$$

SCHEME 1. **Reaction of H/D exchange and its different steps.** k and k_{out} can be deduced as described in Ref. 19.

for optimal functioning of the enzyme. For clarity under "Results," hereafter we qualify T18V, T18Q, T18G, and T18D variants as "poorly active."

A Protonatable Residue at the Small Subunit 18-position Is Not Required for Active Site Chemistry—To test whether the effects of the mutations are caused by the active site chemistry being impaired, we used HDE measurements whereby the enzyme uses protons from the solvent to transform D_2 into HD and then H_2. The course of the reaction is monitored by using mass spectrometry to follow the concentrations of D_2, HD, and H_2 as a function of time. The data can be analyzed to calculate the rate of H_2 diffusion from the active site (k_{out}) and the first order rate constant of HD exchange at the active site (k), which is an indicator of PT and H_2 splitting recombination at the active site (19, 25) (see Scheme 1).

Table 2 shows that the value of k_{out} is similar for the WT and T18S enzymes. The value of k_{out} cannot be determined in the T18V and T18Q variants because the HDE activity is too low. The T18G mutation increases k_{out} 1.5-fold, and the T18D mutation decreases k_{out} about 5-fold. The values of the rate constant k for the T18S and T18D variants are, respectively, ~100 and 10% that measured with WT. In the T18V and T18Q variants, k is <1% that of the value the WT. These results are in line with the H_2 oxidation and proton reduction activities, suggesting defects in proton transfer. However, the T18G variant clearly stands apart as it is practically unable to oxidize and produce H_2, but it catalyzes HDE at a high rate (40% that of the WT).

These results clearly show that the loss of activity provoked by exchanging Thr-18^S with a non-protonatable residue is not necessarily the consequence of impaired proton transfer. Because the above kinetic data are insufficient to identify which step(s) is (are) affected by the mutations, we undertook a spectroscopic and structural characterization of the variants.

The Classical NiC Signature Is Either Undetected or Modified in the Variants That Have Low H_2 Oxidation/Production Activity—We investigated the effects of the mutations on the paramagnetic properties of the [NiFe] active site. After purification in air, the EPR spectrum of the WT shows a mixture of the NiA ($g_{z,y,x}$ = 2.312, 2.230, 2.00) and NiB ($g_{z,y,x}$ = 2.335, 2.155, 2.004) signals (22) (Fig. 3*A*). The amount of nickel species corresponds to 20–80% that of total nickel, depending on the enzyme preparation, the remaining nickel being EPR-silent (37). The ratio of NiB over NiA also strongly varies between preparations (37). The variants we studied displayed the NiA and NiB signals (accounting for 15–80% total nickel) with small changes in the g values (Fig. 3*A*). We performed a redox titration of these inactive states with samples of the T18G and T18D

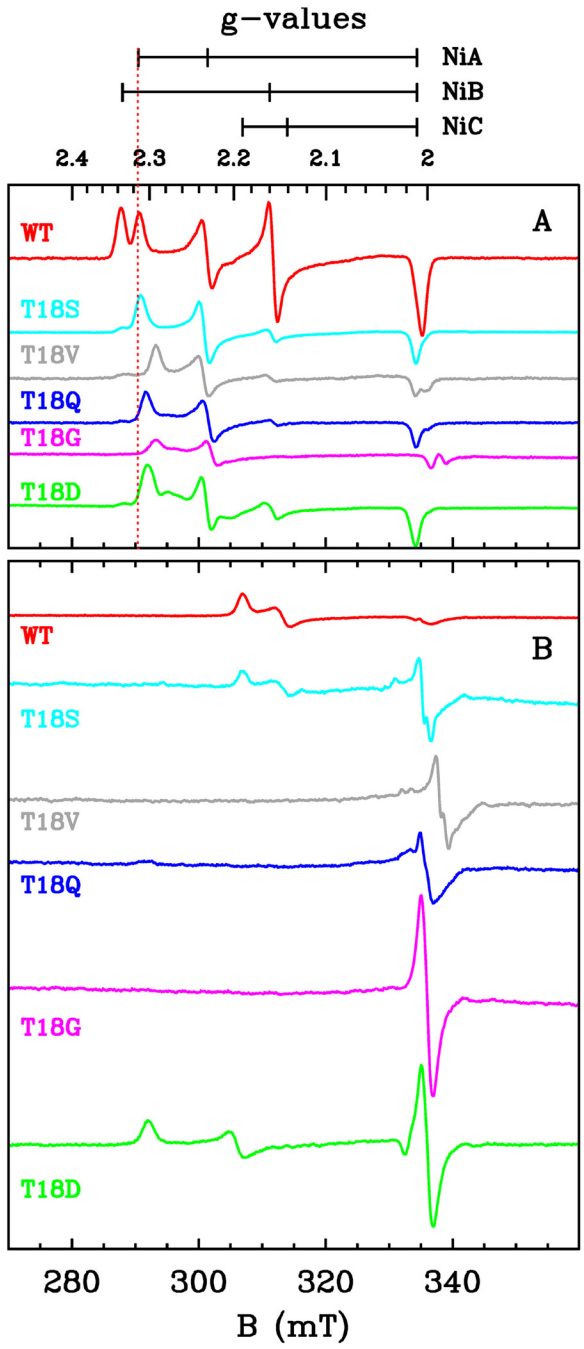

FIGURE 3. **EPR spectra of nickel of Thr-18^S variants in the air-purified (*A*) and dithionite-reduced (*B*) states.** The EPR spectra were recorded at T = 100 K, microwave frequency (ν) = 9.4135 GHz, modulation amplitude (MA) = 1 mT, microwave power (P) = 10 mW, number of scans = 4 (WT, T18D, T18Q) or 9 (T18S, T18V) (*A*) and T = 30 K, ν = 9.4069 GHz, MA = 1 mT, P = 10 mW, number of scans = 1 (WT), 7 (T18D), 8 (T18S, T18G, T18V), or 9 (T18Q) (*B*).

variants (Table 3). The NiA species of the T18G variant has a reduction potential of −90 ± 20 mV, slightly higher than that measured with the WT. In the case of the T18D variant, the signatures of the active site (NiA and NiB species) disappear upon reduction at potential values (−160 ± 20 mV and −120 ± 20 mV, respectively, Table 3) that are similar to those measured with WT (−160 ± 20 mV for both species) (38). In this variant we observed another nickel signal with lines at $g_{z,y}$ = 2.30 and 2.26 and accounting for <5% of the

TABLE 3
Redox potentials of Ni and FeS clusters in the T18D and T18G variants
All values are in mV/standard hydrogen electrode ± 20 mV.

Enzyme	NiA	NiB	[3Fe4S]	2[4Fe4S]
WT[a]	−160	−120	+65	−340
T18G	−90	ND[b]	+25	−330
T18D	−160	−120	+50	−370

[a] From Liebgott *et al.* (38).
[b] The intensity of the NiB signal in the T18G variant was too low to be followed in redox titrations.

enzyme (Fig. 3*A*). This minor Ni(III) species disappears below −320 mV.

Upon reduction of the WT enzyme with dithionite, the NiA and NiB signatures vanish, and the standard NiC rhombic signal ($g_{z,y,x}$ = 2.189, 2.145, 1.996) grows (Fig. 3*B*) (22). This signature amounts to up to 50% that of the total nickel depending on the reductive treatment. The T18S variant also exhibits this typical signal, which we could not detect in the T18V, T18Q, and T18G variants. In the T18D variant, no NiC signal was detected, but we observed a low intensity nickel species at g = 2.30, 2.19, and 2.02 that appears below −320 mV (Fig. 3*B*). This minor nickel species is completely reduced under −361mV. Another low intensity nickel species at g = 2.30 and 2.19 appears below −327mV.

The Redox Properties of the FeS Clusters Are Not Affected by the Mutations—We studied the effect of the mutations on the redox properties of the FeS clusters of the as-prepared and reduced enzymes by EPR spectroscopy. In the air-purified WT and all the mutant enzymes, the medial $[3Fe4S]^{+}$ cluster is paramagnetic (S = ½) and shows up as a weakly anisotropic signal centered on g = 2.02, accounting for 1 spin per molecule (Fig. 4*A*). After dithionite reduction, the two $[4Fe4S]^{+}$ clusters are paramagnetic (S = ½) and magnetically interact together and with the medial iron-sulfur cluster at 6 K, which results in a large and complex signal that develops between 3000 and 4500 G (Fig. 4*B*) in addition to a large signal at low field (approximatively 1500 G), corresponding to the reduced, medial $[3Fe4S]^{0}$ (S = 2). We also observed a magnetic interaction between the proximal $[4Fe4S]^{+}$ and NiC, whose signal splits and shows major features at g = 2.21 and 2.10 (Fig. 4*B*) (39). In all variants we observed the large and complex signature of the $[4Fe4S]^{+}$ clusters, in some cases with small differences that may come from different levels of reduction of the variants (Fig. 4*B*). In the T18S variant, the magnetic interactions between NiC and the proximal cluster are similar to those observed with WT. The T18D variant also shows an interaction spectrum between the reduced nickel species ($g_{z,y,x}$ = 2.30, 2.19, 2.02) and the proximal cluster (Fig. 4*B*). In the T18G and T18D variants, the reduction potentials of the medial [3Fe4S] (around +50 mV) and proximal and distal [4Fe4S] (around −350 mV) clusters are similar to those of the WT (Table 3). These results show that the redox properties of the FeS clusters look the same in all variants and suggest that electron transfer is unaffected in the variants.

The HDE-active T18G Variant Shows a NiR Signal—We investigated the effect of the mutations on the structural/redox properties of the active site of the as-prepared and H_2-treated enzymes by FTIR. The diatomic ligands CO and CN^{-} of the

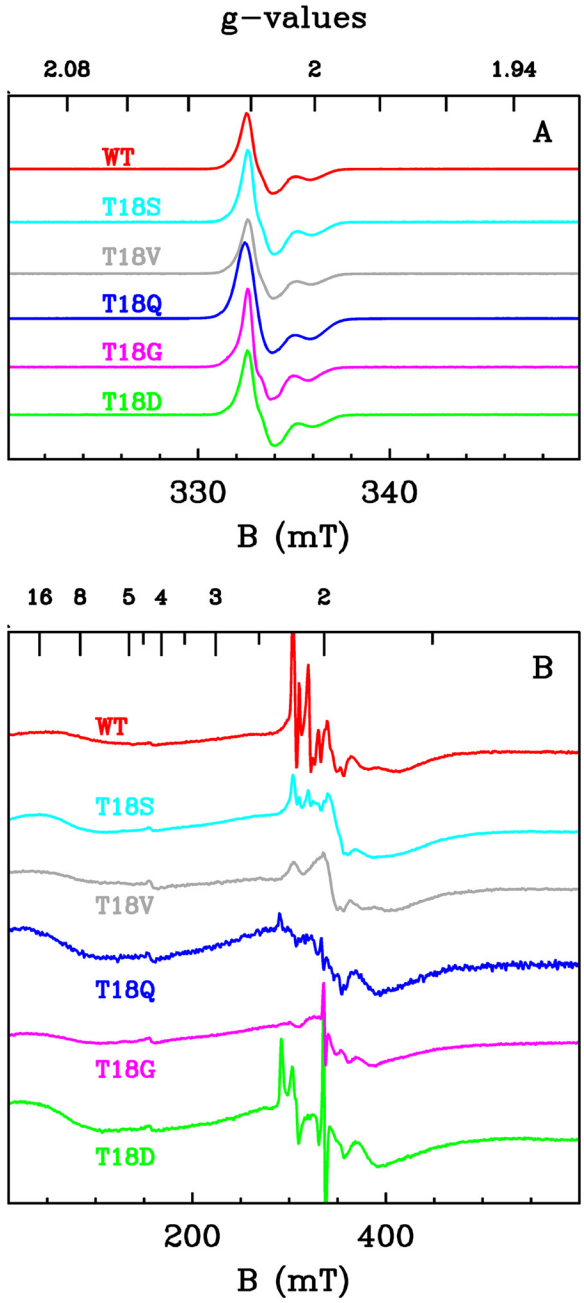

FIGURE 4. **EPR spectra of FeS clusters of the Thr-18^{S} variants.** Medial [3Fe4S] cluster in the air-purified enzymes (*A*) and [4Fe4S] clusters in the dithionite-reduced enzymes (*B*) are shown. The EPR spectra were recorded at T = 15 K, ν = 9.4069 GHz, modulation amplitude (MA) = 0.5 mT (WT, T18Q, T18V) or 0.2 mT (T18S, T18D, T18G), P = 0.4 mW (WT, T18Q, T18V) or 0.1 mW (T18S, T18D, T18G), number of scans = 1 (A) and T = 6 K, ν = 9.4069 GHz, MA = 1 mT, P = 10 mW, number of scans = 1 (WT, T18Q), 4 (T18D, T18G), 10 (T18S, T18V) (*B*).

active site iron atom can be detected by infrared spectroscopy in the 1900–2100-cm^{-1} region. Regarding the WT, each redox state of the active site shows up as a specific set of three IR bands (1 CO and 2 CN^{-} ligands) (2). The spectrum of the air-purified WT enzyme is composed of a mixture of NiA (bands at 1947, 2096, and 2084 cm^{-1}) and NiB (1946, 2080, and 2091 cm^{-1}) and another presumably inactive state also present in preparations of several WT hydrogenases. The latter state is characterized by a CO band at 1911 cm^{-1} and two CN^{-} bands at 2059

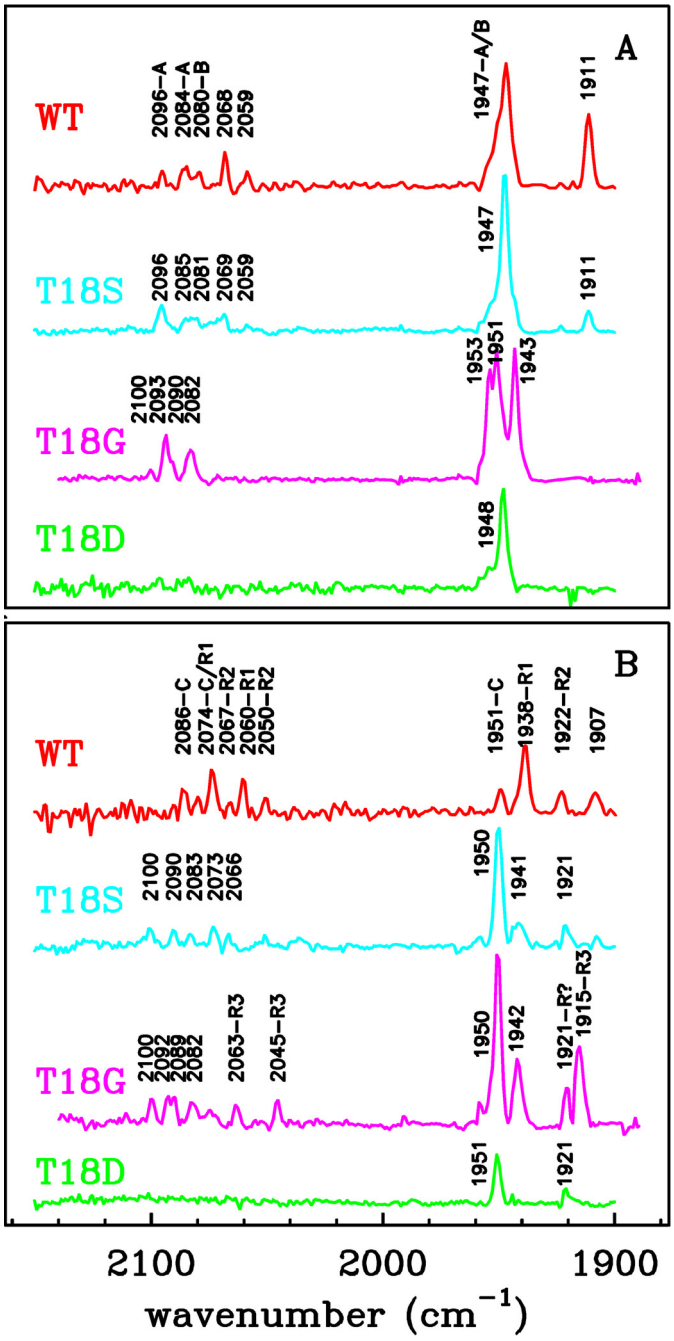

FIGURE 5. **FTIR spectra of WT and Thr-18^S variants from *D. fructosovorans* [NiFe]-hydrogenase as isolated (*A*) or reduced under 1 atm H_2 for 4 h at room temperature (*B*).** The concentrations are 50 μM WT enzyme, 220 μM T18S, 90 μM T18D, 160 μM T18G. For WT, the CO and CN^- bands are labeled as follows: NiA (*-A*), NiB (*-B*), NiC (*-C*), NiR_I (*-R1*), and NiR_{II} (*-R2*). The CN^- band at 2090 cm^{-1} of NiB of WT has too low intensity to be detected. For T18G, the CO and CN^- bands of the state assigned to NiR_{III} are labeled *-R3*, and the CO band of the NiR-like state is labeled *-R?*.

and 2068 cm^{-1} (7, 38, 40), whose intensity varies from one preparation to another (Fig. 5*A*). The signal was recently assigned to a persulfide containing state called Ni-S_{ox} (41). After exposure to H_2 for 4 h, the active site is reduced, and a mixture of the bands of the states NiC (1951, 2074, and 2086 cm^{-1}) and NiR (NiR_I (1938, 2060, and 2074 cm^{-1}) and NiR_{II} (1922, 2051, and 2067 cm^{-1})) is observed (Fig. 5*B*). In line with the results obtained by EPR spectroscopy, the T18S variant behaved similarly to the WT (Fig. 5, *A* and *B*) with the NiA state predominating in the aerobically purified enzyme and a minor contribution of the 1911 cm^{-1} band. Upon H_2 reduction, the bands of NiR and NiC were detected, but the frequencies of the CN^- bands of the NiC state (2100 and 2090 cm^{-1}) were significantly different from those of the WT enzyme (2086 and 2074 cm^{-1}). This difference may be related to the lower H_2 oxidation and production activities of the mutant (50% of the WT).

The spectrum of the air-isolated T18Q variant is similar to that of WT. This variant cannot be reduced by H_2; the CO bands are unchanged after H_2 treatment (data not shown). This is consistent with the absence of NiC noted in the EPR experiments. Note, however, that the NiA and NiB signatures disappear and that the FeS clusters are reduced upon reduction of this variant by dithionite as shown by EPR (see above). The results suggest that H_2 hardly reacts with the active site of this variant and concurs with the very small H_2 oxidation/production and HDE activities measured. The T18V poorly active variant was not characterized by FTIR.

Surprisingly, we could not detect the CN^- bands in the T18D sample either before or after exposure to H_2 (Fig. 5*B*). However, the CO bands are similar to those of the WT and T18S enzymes. Although crystallography shows that the active site structure of the variant is intact (including the three diatomic ligands; see below), the T18D mutation has apparently modified the vibrational properties of the CN^- ligands, decreasing the intensity of their FTIR bands to the noise level of the spectrum. This is in accordance with the modified EPR signatures of this variant whose HDE and H_2 oxidation/reduction activities are 10–20% those of the WT enzyme.

The spectra of the aerobically purified and H_2-treated T18G samples are very different from those obtained with the WT enzyme. After aerobic purification, the FTIR spectrum revealed three enzyme forms with CO bands at 1943, 1951, 1953 cm^{-1} (Fig. 5*A*). Only 4 CN^- bands (instead of 6) could be detected at 2082, 2090, 2093, and 2100 cm^{-1}, suggesting that some bands overlap. The CO bands at 1951 and 1943 cm^{-1} were still present after H_2 treatment (wavenumbers 1950 and 1942 cm^{-1}, respectively), although they were smaller, suggesting that the corresponding enzyme forms are only partially reduced (Fig. 5*B*). In accordance with this, the CN^- bands at 2100, 2092, 2090, and 2082 cm^{-1} were still present. The enzyme form with the CO band at 1953 cm^{-1} was probably the NiA state, which is detected with slightly modified g values in EPR experiments. This form disappeared upon H_2 reduction and was converted into two forms, one of which (with bands at 1915, 2045, 2063 cm^{-1}) is reminiscent of the NiR_{III} state observed in the enzyme from *A. vinosum* (1913, 2043, 2058 cm^{-1}) and *D. vulgaris* (1919, 2050, 2065 cm^{-1}) (2, 7). The other, with a CO band at 1921 cm^{-1}, may be a NiR-like state, but we could not detect the corresponding CN^- bands. One or both of these two reduced states are probably associated with the 40% HDE activity measured for this variant whose H_2 oxidation/production activities is severely impaired.

The Hydrogen-bond Network around the Active Site Was Disrupted in T18D, T18V, and T18G Variants—To analyze the effect of the mutations on the structure of the active site and its protein environment, we solved the structures of the aerobi-

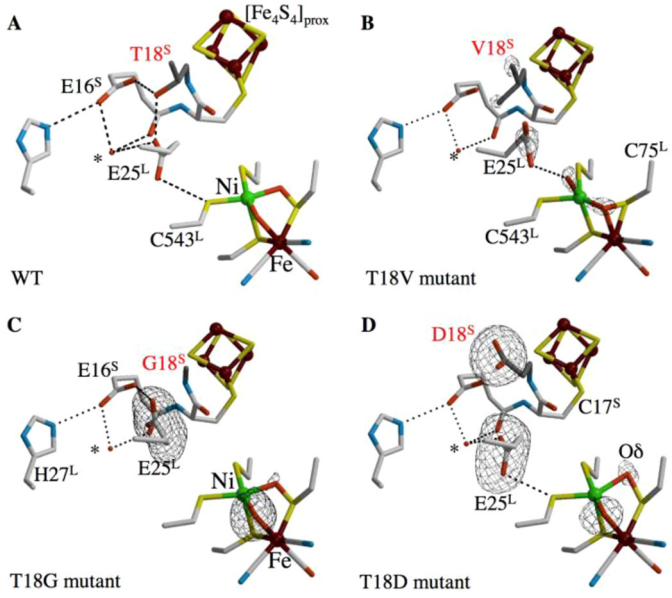

FIGURE 6. **Zoom around Glu-25^L in the crystal structures of WT *D. fructosovorans* [NiFe]-hydrogenase (*A*) and of three aerobically purified Thr-18^S variants (*B–D*).** For the latter, 3-fold averaged omit maps are included (with contour levels of 5 σ in T18V, 7 σ in T18G, and 5 σ in T18D), showing three different conformations for Glu-25^L and a modified NiA structure in the T18V variant due to the stabilization of a terminally bound water ligand to the nickel by the rearranged carboxylate group of Glu-25^L. The * indicates a conserved water molecule. *Dashed lines* indicate putative H-bonding interactions.

cally purified T18V, T18G, and T18D variants at 2.3, 1.95, and 2.6 Å resolutions, respectively (Fig. 6, Table 1). In these structures, the active site and FeS clusters are correctly formed, in agreement with the spectroscopic UV/visible characterization described under "Experimental Procedures" and the EPR results. We focused on the modifications caused by the mutations of the H-bond network; in the WT (Fig. 6*A*), this involves a nickel thiolate-ligand (Cys-543^L), the two oxygen atoms of the carboxylate group of Glu-25^L, and either the alcohol group of Thr-18^S or a water molecule, which are both H-bonded to the carboxylate group of Glu-16^S (Fig. 6*A*). The latter group is also H-bonded to His-27^S via one O atom, and it is within 4 Å from the carboxylate group of Glu-75^S via the other O atom (Fig. 2*A*). Note that Cys-543^L, Glu-25^L, Thr-18^S, Glu-16^S, His-27^L, and Glu-75^S are part of putative proton pathways (13, 14, 16). In the T18V and T18G variants (Fig. 6, *B* and *C*), the side chain of Glu-25^L is rearranged, leading to the loss of the H-bond between Cys-543^L and Glu-25^L and disrupting the first proton transfer step from Cys-543^L. In the T18V variant, a water molecule that is terminally bound to the nickel ion stabilizes the new conformation of Glu-25^L (Fig. 6*B*). In the T18D variant, the side chain of the position-18 residue is moved away from the active site (Fig. 6*D*) and forms H-bonds with His-13^S, Thr-21^S, and Thr-47^S (not shown); it is not H-bonded to Glu-25^L, whose position is the same as in the WT enzyme. Notably, the Glu-16^S putative proton relay (Fig. 2*A*) between the residue in position 18^S and Glu-75^S is short-cut, but a conserved water molecule might also be used for proton transfer between Glu-25^L and Glu-16^S (14). All variants contain a significant fraction of Cys-75 in the oxidized sulfenate form that has recently been assigned to the unready NiA and NiSU states (41). The different sulfenate conformation in T18V might explain the different NiA EPR signal that is observed for this variant (Fig. 3*A*).

DISCUSSION

The catalytic cycle of hydrogenases involves many different steps, including gas transport, long range electron and proton transfer, and active site chemistry (Fig. 1*B*). Many kinetic, spectroscopic, and structural techniques are available to characterize these enzymes, but except for gas transport (19, 24, 25), there is no tool allowing the direct measurement of the rates of the individual steps. Each technique provides useful but only fragmented and indirect information, and ingenious approaches have to be used to learn about the rates of individual steps in the catalytic cycle based on a global measurement of turnover rate (29, 42). In this paper we have carried out an extensive study of several variants using a combination of techniques to assess the role of the position-18 residue in the small subunit of the *Df* [NiFe]-hydrogenase. Except for T18S, the Thr-18^S mutations that we studied have severe effects on both H_2 oxidation and production activities, indicating an important role of the alcohol function of position 18. We used the non-redox HDE assay to show that changing the residue at this position may moderately affect the rate of gas diffusion in the tunnel (Table 2, for example, the rate constant for H_2 release from the active site in the T18D variant is approximatively 5-fold lower than that in the WT enzyme). Because the H_2 oxidation/production rates and the rates of H/D exchange (k) are affected to the same extent in the T18V, T18Q, and T18D variants, it may have been tempting to assume that Thr-18^S is involved in a step that is involved in the three reactions, namely active site chemistry or proton transfer, as suggested by calculations and crystallographic studies (13–16). However, a crucial observation is that the T18G variant is almost inactive for H_2 oxidation or production and yet catalyzes HDE at a high rate. Therefore, the absence of correlation between the rates of H_2 oxidation/production and HDE challenges the conclusion that Thr-18^S is involved in proton transfer. This phenotype of the T18G variant is reminiscent of that of the D15H variant of the sensor hydrogenase from *R. eutropha* for which the authors suggested that electron transfer between the active site and the proximal FeS is impaired (23). Thus, attributing a role to Thr-18^S based on the turnover rates of the variants is not straightforward, and we have expanded the study by a spectroscopic and structural examination of the enzymes to analyze the effect of the mutations on the properties of the redox centers, including the active site.

We have measured or estimated the reduction potentials of the three FeS clusters in the T18G and T18D variants using redox titrations followed by EPR. We could detect no difference with the WT enzyme, suggesting that electron transfer through the chain of FeS clusters is not impaired in the variants (although we cannot rule out the possibility that the mutations have affected other important parameters such as the inner and outer sphere contributions to the reorganization energy or details of the electron tunneling pathways; Ref. 43). However, we have observed that the mutations affect the spectroscopic and structural properties of the active site.

Indeed, the most striking effect of the mutations is a major change in the EPR features of nickel and the FTIR signatures of the active site in the reduced state. Most significantly, in both EPR and FTIR experiments, none of the poorly active variants exhibits the classical NiC signal after reductive treatment. The behavior of the HDE active T18G variant is heterogeneous. A significant fraction of the active site of this variant can be reduced by H_2 to yield states reminiscent of the classical reduced states (NiR), but the NiC state could not be detected. Thus, from the combination of kinetic and spectroscopic characterization of this series of Thr-18^S variants, we could correlate for the first time the detection of NiC with the H_2 oxidation/production activity and the observation of the NiR state with the HDE activity. These results support the proposed catalytic cycle drawn in Fig. 1*B*, and the phenotypes of the Thr-18^S variants can now be simply rationalized: (i) the T18D mutation modifies the redox properties of the reduced states (detected by EPR and FTIR spectroscopies) of the active site which, becomes less efficient for catalysis (10–20% of the turnover rate of the WT enzyme), (ii) the active site of T18Q (and most probably T18V) cannot be reduced into the active NiR and NiC states so that the variants have very low activity (HDE is particularly slow), and (iii) the T18G mutation partially preserves NiR-NiSI interconversion, allowing HDE activity, but prevents NiR-NiC interconversion, making the enzyme unable to quickly turnover H_2.

This interpretation is fully supported by the x-ray data, which show that the T18D, T18V, and T18G mutations induce structural changes around the nickel. Although the structures were determined using samples of the enzymes purified in air, the rupture or disruption of the H-bond network linking nickel to the residue at the 18-position seems detrimental because the variants have little H_2 oxidation or production activity after reductive treatment. In particular, the H-bonding network connecting nickel, Glu-25^L, and Thr-18^S is interrupted because Glu-25^L is displaced in the T18V and T18G variants. In the T18D variant, the H-bond between Glu-25^L and the 18-position residue is lost. Thr-18^S was proposed to be a relay of PT, next to Glu-25^L (11, 13, 15). Alcoholic residues have frequently been shown, including in [FeFe]-hydrogenases, to act as proton relays or to influence the reactivity of neighboring relay residues (44, 45), but we cannot confirm this function, at least for the *Df* enzyme. On the one hand exchanging this alcohol residue with an acidic one (T18D) preserves the H-bond linking nickel via Cys-543^L to Glu-25^L (Fig. 6*D*) but still impairs the catalytic efficiency of the active site (Table 2). On the other hand, having removed the OH function in the T18G variant only slightly affects the HDE activity of the enzyme (*i.e.* does not prevent PT) but breaks the H-bond network linking nickel to the first relay Glu-25^L as shown in the structure of as-prepared enzyme. It may be that a water molecule, not detected in the structure of the air-oxidized enzyme, is incorporated in the enzyme upon activation so that a proton pathway is reconstituted and allows HDE. But even if that were the case, the fact is that the T18G variant is unable to catalyze H_2 oxidation and production. In consequence, our study rather suggests an important role of the alcoholic function of Thr-18^S in maintaining a local active site structure that ensures fast electron and proton transfers involved in the NiSI-NiC-NiR interconversions during redox catalysis.

Acknowledgments—We thank the Pôle de Compétitivité Capénergies and the FrenchBIC research network for support. We thank the staff at the used SLS and ESRF beamlines for assistance with x-ray data collections. We acknowledge the Aix-Marseille EPR spectroscopy Facility Center (national TGE-RENARD network, FR3443) and the HélioBiotec platform (Commissariat à l'Energie Atomique et aux Energies Alternatives (CEA)).

REFERENCES

1. Hatchikian, C. E., Traore, A. S., Fernandez, V. M., and Cammack, R. (1990) Characterization of the nickel-iron periplasmic hydrogenase from *Desulfovibrio fructosovorans*. *Eur. J. Biochem.* **187,** 635–643
2. De Lacey, A. L., Fernandez, V. M., Rousset, M., and Cammack, R. (2007) Activation and inactivation of hydrogenase function and the catalytic cycle: spectroelectrochemical studies. *Chem. Rev.* **107,** 4304–4330
3. Shafaat, H. S., Rüdiger, O., Ogata, H., and Lubitz, W. (2013) [NiFe] hydrogenases: a common active site for hydrogen metabolism under diverse conditions. *Biochimica. et Biophysica. Acta.* **1827,** 986–1002
4. Lubitz, W., Reijerse, E., and van Gastel, M. (2007) [NiFe] and [FeFe] hydrogenases studied by advanced magnetic resonance techniques. *Chem. Rev.* **107,** 4331–4365
5. Bruschi, M., Tiberti, M., Guerra, A., and De Gioia, L. (2014) Disclosure of key stereoelectronic factors for efficient H_2 binding and cleavage in the active site of [NiFe]-hydrogenases. *J. Am. Chem. Soc.* **136,** 1803–1814
6. de Lacey, A. L., Hatchikian, E. C., Volbeda, A., Frey, M., Fontecilla-Camps, J. C., and Fernandez, V. M. (1997) Infrared-spectroelectrochemical characterization of the [NiFe] hydrogenase of *Desulfovibrio gigas*. *J. Am. Chem. Soc.* **119,** 7181–7189
7. Bleijlevens, B., van Broekhuizen, F. A., De Lacey, A. L., Roseboom, W., Fernandez, V. M., and Albracht, S. P. (2004) The activation of the [NiFe]-hydrogenase from *Allochromatium vinosum*: an infrared spectro-electrochemical study. *J. Biol. Inorg. Chem.* **9,** 743–752
8. Pardo, A., De Lacey, A. L., Fernández, V. M., Fan, H. J., Fan, Y., and Hall, M. B. (2006) Density functional study of the catalytic cycle of nickel-iron [NiFe] hydrogenases and the involvement of high-spin nickel(II). *J. Biol. Inorg. Chem.* **11,** 286–306
9. Roessler, M. M., Evans, R. M., Davies, R. A., Harmer, J., and Armstrong, F. A. (2012) EPR spectroscopic studies of the Fe-S clusters in the O_2-tolerant [NiFe]-hydrogenase Hyd-1 from *Escherichia coli* and characterization of the unique [4Fe-3S] cluster by HYSCORE. *J. Am. Chem. Soc.* **134,** 15581–15594
10. Greco, C., Fourmond, V., Baffert, C., Wang, P. H., Dementin, S., Bertrand, P., Bruschi, M., Blumberger, J., de Gioia, L., and Léger, C. (2014) Combining experimental and theoretical methods to learn about the reactivity of gas-processing metalloenzymes. *Energy Environ. Sci.* **7,** 3543–3573
11. Volbeda, A., Charon, M. H., Piras, C., Hatchikian, E. C., Frey, M., and Fontecilla-Camps, J. C. (1995) Crystal structure of the nickel-iron hydrogenase from *Desulfovibrio gigas*. *Nature* **373,** 580–587
12. Ogata, H., Hirota, S., Nakahara, A., Komori, H., Shibata, N., Kato, T., Kano, K., and Higuchi, Y. (2005) Activation process of [NiFe] hydrogenase elucidated by high-resolution x-ray analyses: conversion of the ready to the unready state. *Structure* **13,** 1635–1642
13. Teixeira, V. H., Soares, C. M., and Baptista, A. M. (2008) Proton pathways in a [NiFe]-hydrogenase: a theoretical study. *Proteins* **70,** 1010–1022
14. Fdez Galván, I., Volbeda, A., Fontecilla-Camps, J. C., and Field, M. J. (2008) A QM/MM study of proton transport pathways in a [NiFe] hydrogenase. *Proteins* **73,** 195–203
15. Volbeda, A., Amara, P., Darnault, C., Mouesca, J. M., Parkin, A., Roessler, M. M., Armstrong, F. A., and Fontecilla-Camps, J. C. (2012) X-ray crystallographic and computational studies of the O_2-tolerant [NiFe]-hydrogenase 1 from *Escherichia coli*. *Proc. Natl. Acad. Sci. U.S.A.* **109,** 5305–5310
16. Sumner, I., and Voth, G. A. (2012) Proton transport pathways in [NiFe]-

hydrogenase. *J. Phys. Chem. B.* **116,** 2917–2926
17. Szori-Doroghazi, E., Maróti, G., Szori, M., Nyilasi, A., Rákhely, G., and Kovács, K. L. (2012) Analyses of the large subunit histidine-rich motif expose an alternative proton transfer pathway in [NiFe] hydrogenases. *PLoS ONE* **7,** e34666
18. Cammack, R., Frey, M., and Robson, R. (2001) *Hydrogen as a Fuel, Learning from Nature*, pp. 77–80, Taylor and Francis, New York
19. Abou-Hamdan, A., Dementin, S., Liebgott, P. P., Gutierrez-Sanz, O., Richaud, P., De Lacey, A. L., Rousset, M., Bertrand, P., Cournac, L., and Léger, C. (2012) Understanding and tuning the catalytic bias of hydrogenase. *J. Am. Chem. Soc.* **134,** 8368–8371
20. Yagi, T., Ogo, S., and Higuchi, Y. (2014) Catalytic cycle of cytochrome-c3 hydrogenase, a [NiFe]-enzyme, deduced from the structures of the enzyme and the enzyme mimic. *Int. J. Hydrogen Energy* **39,** 18543–18550
21. Yagi, T., and Higuchi, Y. (2013) Studies on hydrogenase. *Proc. Jpn. Acad.* **89,** 16–33
22. Dementin, S., Burlat, B., De Lacey, A. L., Pardo, A., Adryanczyk-Perrier, G., Guigliarelli, B., Fernandez, V. M., and Rousset, M. (2004) A glutamate is the essential proton transfer gate during the catalytic cycle of the [NiFe] hydrogenase. *J. Biol. Chem.* **279,** 10508–10513
23. Gebler, A., Burgdorf, T., De Lacey, A. L., Rüdiger, O., Martinez-Arias, A., Lenz, O., and Friedrich, B. (2007) Impact of alterations near the [NiFe] active site on the function of the H_2 sensor from *Ralstonia eutropha*. *FEBS. J.* **274,** 74–85
24. Liebgott, P. P., Leroux, F., Burlat, B., Dementin, S., Baffert, C., Lautier, T., Fourmond, V., Ceccaldi, P., Cavazza, C., Meynial-Salles, I., Soucaille, P., Fontecilla-Camps, J. C., Guigliarelli, B., Bertrand, P., Rousset, M., and Léger, C. (2010) Relating diffusion along the substrate tunnel and oxygen sensitivity in hydrogenase. *Nat. Chem. Biol.* **6,** 63–70
25. Leroux, F., Dementin, S., Burlat, B., Cournac, L., Volbeda, A., Champ, S., Martin, L., Guigliarelli, B., Bertrand, P., Fontecilla-Camps, J., Rousset, M., and Léger, C. (2008) Experimental approaches to kinetics of gas diffusion in hydrogenase. *Proc. Natl. Acad. Sci. U.S.A.* **105,** 11188–11193
26. Rousset, M., Montet, Y., Guigliarelli, B., Forget, N., Asso, M., Bertrand, P., Fontecilla-Camps, J. C., and Hatchikian, E. C. (1998) [3Fe-4S] to [4Fe-4S] cluster conversion in *Desulfovibrio fructosovorans* [NiFe] hydrogenase by site-directed mutagenesis. *Proc. Natl. Acad. Sci. U.S.A.* **95,** 11625–11630
27. Léger, C., Dementin, S., Bertrand, P., Rousset, M., and Guigliarelli, B. (2004) Inhibition and aerobic inactivation kinetics of *Desulfovibrio fructosovorans* NiFe hydrogenase studied by protein film voltammetry. *J. Am. Chem. Soc.* **126,** 12162–12172
28. Fourmond, V., Baffert, C., Sybirna, K., Dementin, S., Abou-Hamdan, A., Meynial-Salles, I., Soucaille, P., Bottin, H., and Léger, C. (2013) The mechanism of inhibition by H_2 of H_2-evolution by hydrogenases. *Chem. Commun. (Camb)* **49,** 6840–6842
29. Dementin, S., Burlat, B., Fourmond, V., Leroux, F., Liebgott, P. P., Abou Hamdan, A., Léger, C., Rousset, M., Guigliarelli, B., and Bertrand, P. (2011) Rates of intra- and intermolecular electron transfers in hydrogenase deduced from steady-state activity measurements. *J. Am. Chem. Soc.* **133,** 10211–10221
30. Volbeda, A., Garcin, E., Piras, C., De Lacey, A. L., Fernandez, V. M., Hatchikian, C. E., Frey, M., and Fontecilla-Camps, J. C. (1996) Structure of the [NiFe] hydrogenase active site: evidence for biologically uncommon Fe ligands. *J. Am. Chem. Soc.* **118,** 12989–12996
31. Vernède, X., and Fontecilla-Camps, J. C. (1999) A method to stabilize reduced and or gas-treated protein crystals by flash-cooling under a controlled atmosphere. *J. Appl. Crystallogr.* **32,** 505–509
32. Kabsch, W. (2010) Xds. *Acta Crystallogr. D Biol. Crystallogr.* **66,** 125–132
33. McCoy, A. J., Grosse-Kunstleve, R. W., Adams, P. D., Winn, M. D., Storoni, L. C., and Read, R. J. (2007) Phaser crystallographic software. *J. Appl. Crystallogr.* **40,** 658–674
34. Volbeda, A., Martin, L., Cavazza, C., Matho, M., Faber, B. W., Roseboom, W., Albracht, S. P., Garcin, E., Rousset, M., and Fontecilla-Camps, J. C. (2005) Structural differences between the ready and unready oxidized states of [NiFe] hydrogenases. *J. Biol. Inorg. Chem.* **10,** 239–249
35. Murshudov, G. N., Skubák, P., Lebedev, A. A., Pannu, N. S., Steiner, R. A., Nicholls, R. A., Winn, M. D., Long, F., and Vagin, A. A. (2011) REFMAC5 for the refinement of macromolecular crystal structures. *Acta Crystallogr. D Biol. Crystallogr.* **67,** 355–367
36. Emsley, P., Lohkamp, B., Scott, W. G., and Cowtan, K. (2010) Features and development of Coot. *Acta Crystallogr. D Biol. Crystallogr.* **66,** 486–501
37. Dementin, S., Leroux, F., Cournac, L., de Lacey, A. L., Volbeda, A., Léger, C., Burlat, B., Martinez, N., Champ, S., Martin, L., Sanganas, O., Haumann, M., Fernández, V. M., Guigliarelli, B., Fontecilla-Camps, J. C., and Rousset, M. (2009) Introduction of methionines in the gas channel makes [NiFe] hydrogenase aero-tolerant. *J. Am. Chem. Soc.* **131,** 10156–10164
38. Liebgott, P. P., de Lacey, A. L., Burlat, B., Cournac, L., Richaud, P., Brugna, M., Fernandez, V. M., Guigliarelli, B., Rousset, M., Léger, C., and Dementin, S. (2011) Original design of an oxygen-tolerant [NiFe] hydrogenase: major effect of a valine-to-cysteine mutation near the active site. *J. Am. Chem. Soc.* **133,** 986–997
39. Guigliarelli, B., More, C., Fournel, A., Asso, M., Hatchikian, E. C., Williams, R., Cammack, R., and Bertrand, P. (1995) Structural organization of the Ni and (4Fe-4S) centers in the active form of *Desulfovibrio gigas* hydrogenase. Analysis of the magnetic interactions by electron paramagnetic resonance spectroscopy. *Biochemistry* **34,** 4781–4790
40. Abou-Hamdan, A., Burlat, B., Gutiérrez-Sanz, O., Liebgott, P. P., Baffert, C., De Lacey, A. L., Rousset, M., Guigliarelli, B., Léger, C., and Dementin, S. (2013) O_2-independent formation of the inactive states of NiFe hydrogenase. *Nat. Chem. Biol.* **9,** 15–17
41. Volbeda, A., Martin, L., Barbier, E., Gutiérrez-Sanz, O., De Lacey, A. L., Liebgott, P. P., Dementin, S., Rousset, M., and Fontecilla-Camps, J. C. (2015) Crystallographic studies of [NiFe]-hydrogenase mutants: towards consensus structures for the elusive unready oxidized states. *J. Biol. Inorg. Chem.* **20,** 11–22
42. Dementin, S., Belle, V., Bertrand, P., Guigliarelli, B., Adryanczyk-Perrier, G., De Lacey, A. L., Fernandez, V. M., Rousset, M., and Léger, C. (2006) Changing the ligation of the distal [4Fe4S] cluster in NiFe hydrogenase impairs inter- and intramolecular electron transfers. *J. Am. Chem. Soc.* **128,** 5209–5218
43. Marcus, R. A., and Sutin, N. (1985) Electron transfers in chemistry and biology. *Biochim. Biophys. Acta* **811,** 265–322
44. Ginovska-Pangovska, B., Ho, M. H., Linehan, J. C., Cheng, Y., Dupuis, M., Raugei, S., and Shaw, W. J. (2014) Molecular dynamics study of the proposed proton transport pathways in [FeFe]-hydrogenase. *Biochim. Biophys. Acta.* **1837,** 131–138
45. Cornish, A. J., Gärtner, K., Yang, H., Peters, J. W., and Hegg, E. L. (2011) Mechanism of proton transfer in [FeFe]-hydrogenase from *Clostridium pasteurianum*. *J. Biol. Chem.* **286,** 38341–38347

A Threonine Stabilizes the NiC and NiR Catalytic Intermediates of [NiFe]-hydrogenase

Abbas Abou-Hamdan, Pierre Ceccaldi, Hugo Lebrette, Oscar Gutiérrez-Sanz, Pierre Richaud, Laurent Cournac, Bruno Guigliarelli, Antonio L. De Lacey, Christophe Léger, Anne Volbeda, Bénédicte Burlat and Sébastien Dementin

J. Biol. Chem. 2015, 290:8550-8558.
doi: 10.1074/jbc.M114.630491 originally published online February 9, 2015